International Nano Letters (2019) 9:221–229
https://doi.org/10.1007/s40089-019-0274-6

ORIGINAL ARTICLE

Order fluctuation induced tunable light emission from carbon nanosystem

M. S. Swapna[1] · **S. Sankararaman**[1]

Received: 4 December 2017 / Accepted: 17 April 2019 / Published online: 24 April 2019

Abstract

The paper reports the thermal-induced order fluctuations, in a carbon nanosystem with carbon nanotubes (CNTs) synthesized by the incomplete combustion of gingelly oil. The sample annealed at different temperatures (30–400 °C) is subjected to various morphological and spectroscopic characterizations. The ultraviolet–visible spectroscopic and thermogravimetric analyses reveal the CNTs in the sample. The high-resolution transmission electron microscopy (HR-TEM) also confirms the formation of CNTs in the sample. The Raman spectrum and X-ray diffraction pattern show the signature of multi-walled to single-walled CNT transformation and thus an order fluctuation on annealing. The quantum yield of the sample, measured by integrating sphere method, yields 46.15% at an emission wavelength of 575 nm. When the excitation wavelength is varied from 350 to 510 nm, the CIE coordinate moves from the white region to the yellowish-green region. The varying amount of CNTs in the soot, upon annealing is found to vary the luminescence emission from the sample. The study reveals the thermal-induced oscillatory order in carbon nanosystem with carbon nanotubes (CNTs) leading to tunable excitation/thermal-dependent luminescence emission and thereby suggesting the possibility of converting the futile soot for fruitful applications in photonics and nanoelectronics.

Keywords Carbon nanosystem · Single-walled carbon nanotubes · Multi-walled carbon nanotubes · Raman spectroscopy · Thermogravimetric analysis · CIE plot · Quantum yield · Gingelly oil

Introduction

Carbon and its allotropes have become the focus of research during the last 15 years because of their potential applications in electronics and photonics [1–5]. Carbon nanotubes (CNTs) are one of the most elegant arrangements of solid carbon that are elongated structures of C_{60} molecules (fullerenes) [6, 7]. Multi-walled (MW) CNTs consist of concentric cylindrical graphene layers [8, 9]. The high specific surface area makes them suitable for sensor applications. They have better electrical conductivity than copper, exceptional mechanical strength [10] and high flexibility. The strength of nanotubular materials can be increased by assembling them in the form of ropes of 20–30 nm diameter and several micrometers in length [11]. There are several methods of synthesis such as thermal carbonization, sonication, laser irradiation and exfoliation that have been used for synthesizing different carbon nano particle/tubes/fibers [6, 8, 9, 12]. In the present work, we have adopted the traditional method of incomplete combustion of gingelly oil for the synthesis of carbon nanoparticles (CNPs). It is reported that the increase in the amount of CNT in the sample increases the electrical conductivity [13].

Raman scattering and X-ray diffraction (XRD) techniques have become a potential tool in the last 5 decades, with the advent of lasers and data acquisition systems, for the non-destructive structural characterization of materials. For highly ordered crystalline materials, X-ray diffraction techniques are usually used. But for disordered materials such as soot, Raman spectroscopic studies are useful as they are sensitive to both crystalline and short-range molecular structures. It is a well-studied fact that Raman spectrum of graphitic crystals originates from the lattice vibrations, hence the spectrum will be reflecting the order, disorder and the crystallite size [14–16]. Since the samples under investigation are synthesized by incomplete combustion

✉ S. Sankararaman
drssraman@gmail.com

[1] Department of Optoelectronics and Department of Nanoscience and Nanotechnology, University of Kerala, Trivandrum, Kerala 695581, India

of gingelly oil they contain a mixture of amorphous and graphitic carbon. The degree of graphitization and formation of MWCNTs or single-walled (SW) CNTs can be understood from Raman spectroscopic analysis. Raman spectrum of SWCNT and DWCNT (double walled) exhibit three characteristic bands—radial breathing mode (RBM-100–350 cm^{-1}), D mode ~ 1350 cm^{-1} and tangential stretching G mode (~ 1550–1560 cm^{-1}) [17]. In addition, SWCNTs show an intermediate frequency mode (IFM) between 387 and 1200 cm^{-1} [18–20]. Raman spectra of pure crystalline graphite show only one peak at 1580 cm^{-1} called the G band corresponding to E_{2g} symmetry mode of sp^2 carbon. The presence of defects or disorder breaks the crystal symmetry and activates the certain vibration modes called defect or disorder or D band. The D band in amorphous carbon is assigned to double-resonance Raman Effect in sp^2 carbon [21, 22]. From the ratio of the intensities of first-order D band and G band, crystallite size can be calculated. Higher intensity ratio indicates a higher degree of disorder in the nanostructure. These structural variations are capable of inducing variations in the optical emission behaviour of the material.

Carbon and its allotropes possessing exciting luminescence properties have gained attention of researchers due to its ease of processing, biocompatibility, abundance, low cost, and greater stability [23–25]. These properties make it a potential candidate in the development of phosphor-free light emitters [1, 23, 24]. There are several recent reports suggesting the possibility and potential of various allotropes of carbon and soot in optoelectronic applications [26–30]. Photoluminescence spectroscopy is a powerful non-destructive technique for investigating the luminescence properties of materials of all kinds [23]. The perception of the human eye to the emission from a light source, giving out radiations of different wavelength and intensity can be expressed with the help of chromaticity diagram or CIE plot [31, 32]. The power spectrum, CIE coordinates, and colour purity of a material give a better understanding of its luminescence and fluorescence behaviour [1]. This helps in exploring the application of the material as an efficient light source. In this paper, we report the tunable luminescence emission induced by the order–disorder–reorder transitions of carbon systems as a result of annealing and thereby to get a low-cost electrically tunable material for potential applications in nanoelectronics and photonics.

Experimental methods

Carbon nanoparticles are synthesized by the incomplete combustion of gingelly oil. The soot particles collected are powdered in a ball milling unit. The sample is annealed to 400 °C in step of 100 °C at the rate of 3 °C per minute in a tubular furnace in nitrogen atmosphere keeping the sample for 1 h in each step. The sample (T1) annealed at 100 °C, 200 °C, 300 °C, and 400 °C are labelled as T2, T3, T4, and T5 respectively. The samples are then subjected to Raman spectroscopic, XRD, Fourier transform infrared (FTIR), and thermogravimetric analyses (TGA). The ultraviolet (UV)–visible spectrum is recorded using Jasco V550 UV–visible spectrophotometer. The morphological characterization and composition study (Energy-Dispersive Spectroscopy—EDS) of the sample is carried out in Nova Nano Field Emission Scanning Electron Microscopy (FESEM) and JEOL JEM-2100 High-Resolution Transmission Electron Microscopy (HR-TEM). Raman spectrum is recorded using Lab Ram Micro-Raman Spectrometer with Argon ion laser at 514.5 nm wavelength and power of 5 mW as the excitation source. The thermal stability of the sample weighed 2.040 mg is studied using Perkin Elmer thermogravimetric analyzer, heated from 35 to 900°C at a scanning rate of 10°C/min in the nitrogen atmosphere. This gives information regarding the structure of the CNTs. From the Raman spectrum the crystallite size can be calculated by noting the intensity ratio of D and G band. XRD measurements are carried out in Bruker D8 Advanced Diffractometer with CuKα radiation ($\lambda = 1.5406$ Å). The information about the degree of order can be obtained from the intensity ratio of the peaks corresponding to 2θ values at 20° and 25°. FTIR spectrum is recorded in the range 4000–400 cm^{-1} using Thermo Fisher Scientific Nicolet iS50 FT-IR Spectrophotometer in the ATR mode to understand the structure of the sample through vibrational analysis. The luminescence behaviour is studied by recording the photoluminescence (PL) spectrum by Horiba Fluoromax.

Results and discussion

To assess the thermal stability and chemical purity of the sample, it is subjected to TGA analysis. The TGA analysis provides the changes in the physical and chemical properties of the material as a function of increasing temperature. TGA is commonly used to determine certain characteristics of materials that exhibit weight loss or gain due to decomposition or oxidation. The temperature at which the material starts to decompose is known as initiation temperature. At oxidation temperature, maximum weight loss occurs and this temperature indicates the thermal stability of the material [33]. It has been reported that amorphous carbons decompose at lowest temperatures [34, 35] followed by SWCNTs, MWCNTs, and graphitic particles, respectively. Oxidation temperatures for MWCNTs, and SWCNTs are in the range 400–650 °C and 350–500 °C, respectively [17].

The TGA curve of the gingelly oil soot sample at room temperature is shown in Fig. 1. The graph shows a clear

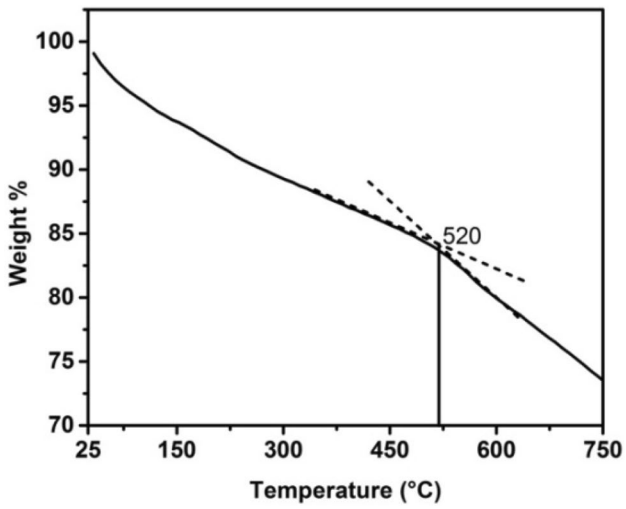

Fig. 1 TGA curve of the sample (T1) at room temperature

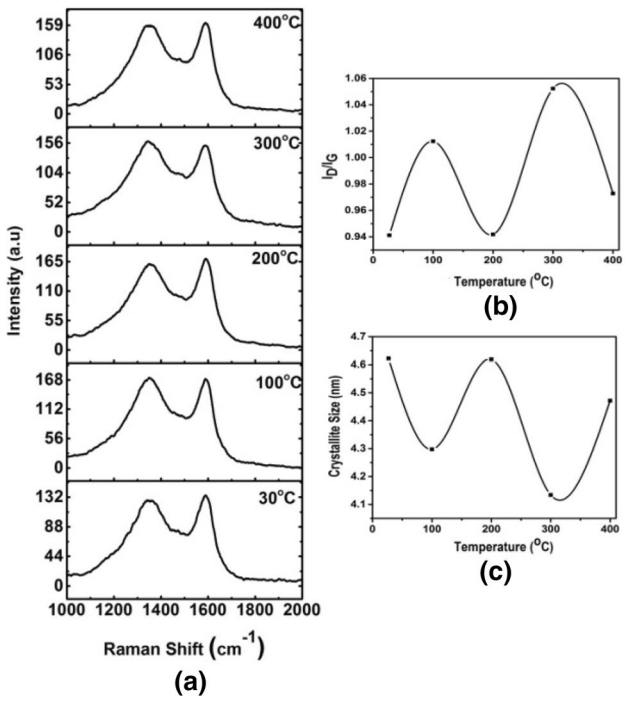

Fig. 2 Raman spectroscopic analysis of the samples T1–T5: (**a**) Raman spectra (**b**) variation of ID/IG ratio (**c**) variation of crystallite size

slope change at 520 °C indicating a structural change. The TGA curve shows a continuous weight loss up to 520 °C. This is because of the fact that the soot sample is a mixture of amorphous carbon, SWCNTs, MWCNTs and graphitic particles. The slope change at 520 °C indicates the presence of MWCNTs and SWCNTs in the sample. MWCNTS are more susceptible to oxidation and undergo decomposition. It is observed that the thinning of MWCNTs occur in a layer by layer fashion [36, 37]. Yao found the decomposition rates of the concentric layers and showed a faster decomposition rate for layers within the nanotube structures. Defects along the walls of the tube may also contribute to the decomposition of MWCNTs by providing initiation sites for the decomposition. The decomposition of the middle layers occurs faster than the interior or exterior layers [38]. Depending on the tube diameter, defects, length, and the number of layers, the decomposition temperature of MWCNTs vary. The decomposition of the MWCNTs with different length and diameter shows a direct relation with annealing temperature [17, 39, 40]. The TGA curve for the sample confirms the decomposition of the MWCNTs in the sample.

The structural information about the sample can be had from Raman spectroscopy. To understand the structural variations occurring in the sample on annealing, Raman spectra recorded in the range 1000–2000 cm^{-1} are shown in Fig. 2. The variation of the intensity ratio of the D and G band (I_D/I_G) and the crystallite size (L) with annealing temperature are shown in Fig. 2b, c, respectively. The samples show D band around 1350 cm^{-1} and G band around 1589 cm^{-1} indicating the presence of CNTs. The planar microcrystalline size (L) for the samples is calculated from the intensities of D and G bands of Raman spectra using Tuinstra and Koening relation [5, 41], $L = 4.35\ (I_G/I_D)$ nm. From Fig. 2b it is evident that the density of defects in the sample, as measured through the ratio of intensities of the D and G band (I_D/I_G), shows a thermal-induced oscillatory behaviour. Upon annealing, it can be seen that the system is moving from an ordered state at room temperature to a less ordered state at 100 °C, and again to an ordered state at 200 °C. The disorder is found to increase further on annealing to 300 °C and decrease at 400 °C. In an amorphous carbon there will be a mixture of sp^3, sp^2, and sp^1 sites. Only E_{2g} mode for graphite and E_1 and E_2 symmetry modes for CNTs is Raman active. When the temperature is increased the conversion of sp^3 bonds to sp^2 bonds, desorption of hydrogen, and conversion of carbon structure to nanocrystalline graphite occur. A similar variation with temperature can also be seen in the crystallite size from Fig. 2c. The thermal-induced oscillation in the crystallite size, obtained from the Raman spectrum is in agreement with the TGA analysis of variations in the dimensions of the MWCNTs in the sample [17, 37, 39, 40, 42].

The Raman spectroscopic analysis of the sample annealed at different temperatures exhibits varying degree of graphitization and the formation of MWCNTs or SWCNTs. The characteristic band exhibited by the Raman spectrum of SWCNT and DW (double walled) CNT is the radial breathing mode (RBM) around 100–400 cm^{-1} [17, 20]. The RBM in the Raman spectrum of the samples (T1–T5) recorded in the range 50–400 cm^{-1} (Fig. 3a) shows a peak around 124 cm^{-1}. The RBM analysis

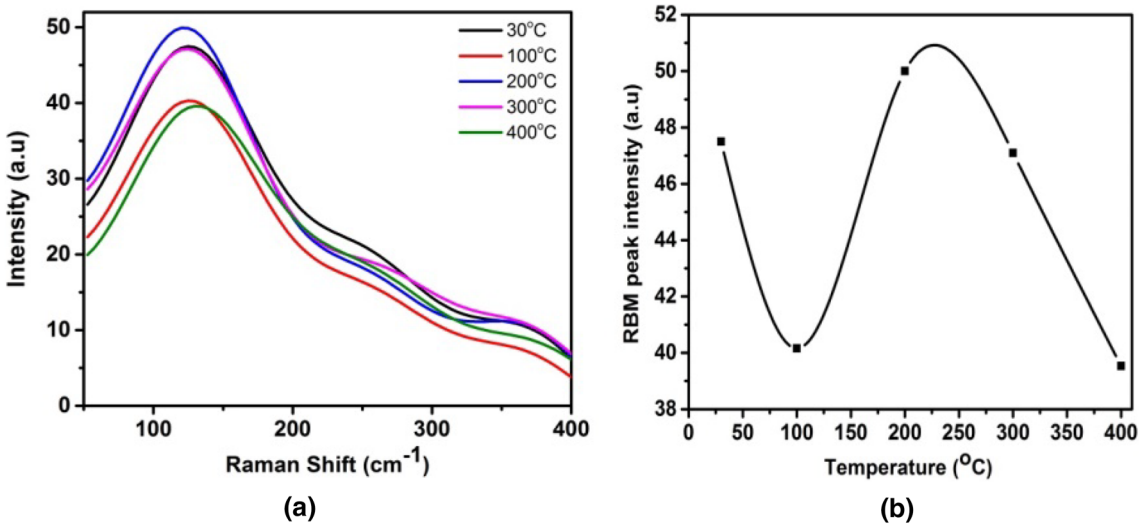

Fig. 3 **a** RBM spectra. **b** Variation of RBM peak intensity with annealing temperature for the samples T1–T5

indicates the presence of SWCNTs of average tube diameter 2 nm which is calculated using the relation $d = 248/\omega$, where ω is the frequency of RBM. The intensity fluctuation of the RBM peak, shown in Fig. 3b, is a clear indication of variation of SWCNTs in the sample.

Another signature of SWCNTs exhibited by the Raman spectrum is the presence of intermediate frequency mode (IFM) between 400 and 1000 cm^{-1} [18, 20]. The IFM of the samples (T1–T5) recorded in the range 600–1000 cm^{-1} (Fig. 4a) shows a broad peak around 833 cm^{-1}. From literature [19, 20, 43] it can be seen that the IFM arises due to the combinational modes of the zone-folded optic and acoustic branches of 2-D graphite and indicates structural defects in SWCNTs. There are also reports of the IFM frequency dependence on tube diameter [19]. Figure 4b, c shows an oscillatory variation in the peak position and intensity of IFM with annealing temperature, similar to that observed in I_D/I_G, crystallite size, RBM, and TGA analyses.

The oscillatory behaviour observed in RBM, IFM, and I_D/I_G (Figs. 2, 3, 4) upon annealing can be considered as the breaking of van der Waals bonds between the layers of MWCNTs leading to the formation of SWCNTs. The increase of temperature results in the thinning of MWCNTs due to the removal of inner layers as reported by Yao [37] and the partial separation of layers of MWCNTs due to van der Waals bond breakage [44] may be the reason for the increase or decrease of disorder evidenced through I_D/I_G ratio variation.

The degree of graphitization and the presence of CNTs can be understood from the X-ray powder diffraction pattern of the samples (T1–T5) recorded in the range $2\theta = 10°–70°$ as shown in the Fig. 5a. The broadened peak around 25° in the XRD pattern is a general feature of all

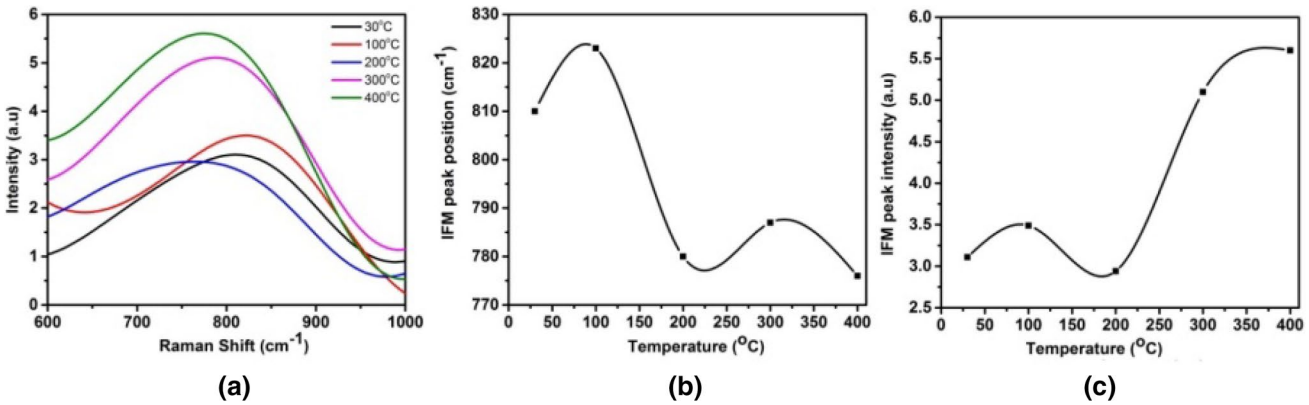

Fig. 4 **a** IFM spectra. **b** Variation of IFM peak position. **c** Variation of IFM peak intensity with annealing temperature for samples T1–T5

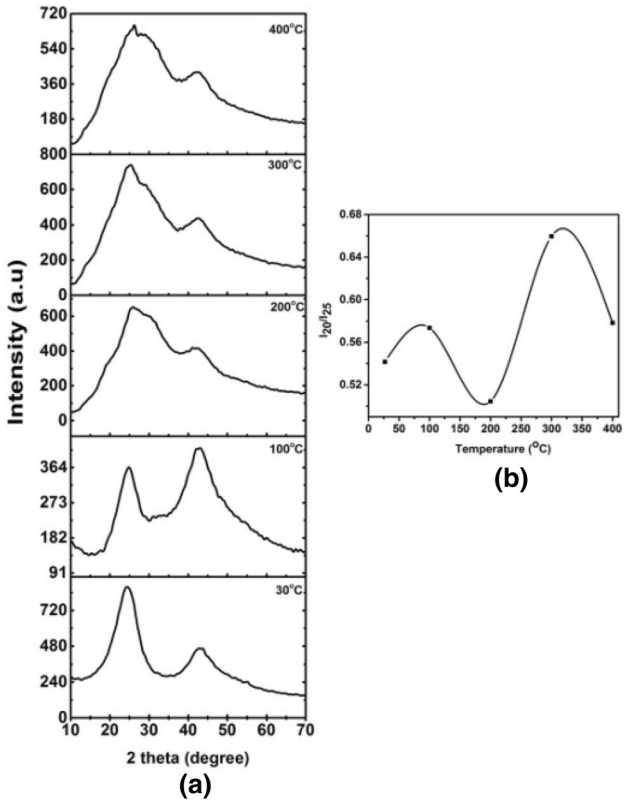

Fig. 5 **a** XRD pattern of samples T1–T5 **b** Variation of I20/I25 with annealing temperature

soot samples which is attributed to the graphitic E_{2g} mode of sp^2-bonded carbon atoms and the ordered CNTs in it [45]. The amorphous carbon and the surface defects of CNTs present in the sample get reflected through the band at 20° which is assigned to the (002) plane and that at 42° to the hexagonal lattice of multi-walled CNT [5, 46, 47]. The quality of CNTs in the sample and the degree of disorder can be understood from the intensity ratio (I_{20}/I_{25}) of the peaks around 20° (I_{20}) and 25° (I_{25}). The smaller the value of intensity ratio the smaller is the degree of disorder in the sample. From Fig. 5b, the variation of I_{20}/I_{25} with annealing temperature, it can be seen that the values of I_{20}/I_{25} are small indicating the sample to be of good quality. The intensities of the peaks at 20° and 25° are obtained through the deconvolution of the broad peak around 25°. It is interesting to note that the order–disorder fluctuations shown in Fig. 5b is in good agreement with that observed in the I_D/I_G ratio from the Raman spectrum as shown in Fig. 2b. The peaks around 42° in Fig. 5a confirm the presence of MWCNTs in the sample which agrees well with the literature. The removal of amorphous carbon up to 200 °C is responsible for the initial decrease of intensity as shown in Fig. 5b. The dynamics of MWCNTs as a result of thinning/shortening/partial separation of layers becomes dominant beyond 200 °C as the system moves to a more ordered state at 400 °C.

The FTIR spectral analysis gives information about the functional groups formed in the soot samples as a result of combustion [33, 48–51]. The FTIR spectra of the sample annealed at different temperatures are given in Fig. 6a. The presence of CNTs is confirmed by the appearance of the peaks at 890, 1104 and 1537 cm^{-1} that are due to the C=C and C=O bonds. The variation in the intensity of the signature peaks of CNTs with annealing temperature is given in Fig. 6b. This also shows a thermal-induced fluctuation as a result of the structural changes occurring in the MWCNTs/SWCNTs present in the soot sample which is also evident from the TGA, Raman, and XRD analyses.

UV–visible spectroscopic analysis of the sample helps to understand the $\pi \rightarrow \pi^*$ transitions of C–C and C=C bonds in sp^2 hybrid regions of the carbon core [21] and the diameter of the SWCNTs by noting the π plasmon resonant absorbance peak. The broad UV–visible absorption spectrum of the sample T1 is shown in Fig. 7a and the tube diameter (d in nm) calculated using the equation $E = 4.80 + (0.70/d^2)$ [52], where E is energy in electron volt (eV) corresponding to the peak at 257 nm is found to be 5.91 nm. The EDX of the sample T1 shown in Fig. 7b shows only carbon and oxygen. Figure 8a–c shows the FESEM and HR-TEM image of the sample T5. The FESEM image confirms the CNPs and the HR-TEM image confirms the presence of CNTs in the soot that supports the XRD, TGA, FTIR, and Raman spectroscopic analysis.

The luminescent properties of the material can be understood from photoluminescence (PL) spectroscopic technique. The PL spectra of the sample at room temperature 30 °C, annealed at 200 °C and 400 °C and recorded in the range 400–800 nm for the excitation wavelengths (λ_{exc}) of 350 nm are shown in Fig. 9 as representative. How human eye perceives the emission from a light source can be expressed with the help of chromaticity diagram or CIE plot [1, 31]. To study the effect of excitation wavelengths on emission pattern, the PL spectra are recorded at 350 nm, 390 nm, 430 nm, and 510 nm. The CIE plot for the sample under different excitation wavelengths and annealing temperature is given in Fig. 10. The trajectory of colour variations with excitation wavelengths (350–510 nm) for the three samples is marked in Fig. 10. For the sample at room temperature and higher temperatures, it can be seen that when the excitation wavelength is increased from 350 to 510 nm, the CIE coordinate moves from the white region to the yellowish-green region. Figure 10a, b, c shows the trajectories of excitation-dependent emissions at 30 °C, 200 °C, and 400 °C. Thus Fig. 10 reveals the excitation- and temperature-dependent tunability of emission from the sample. The order fluctuation, which is evident from the Raman spectrum, XRD pattern, FTIR spectrum, and TGA

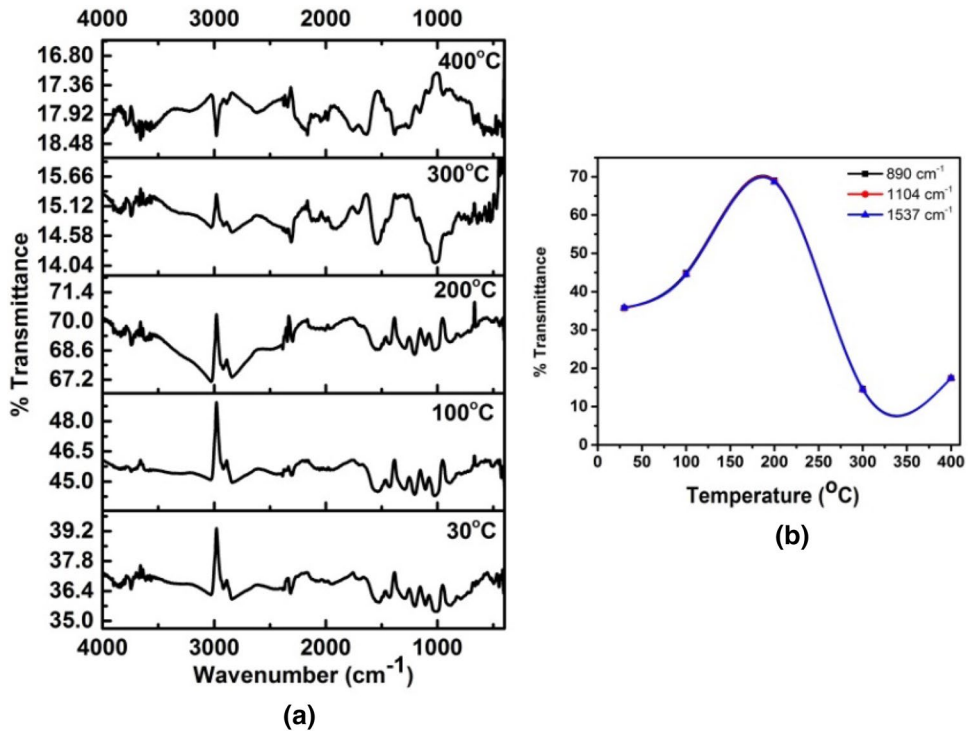

Fig. 6 **a** FTIR spectrum of samples T1–T5. **b** Variation of FTIR peak intensities (890, 1104, and 1537 cm^{-1}) with annealing temperature

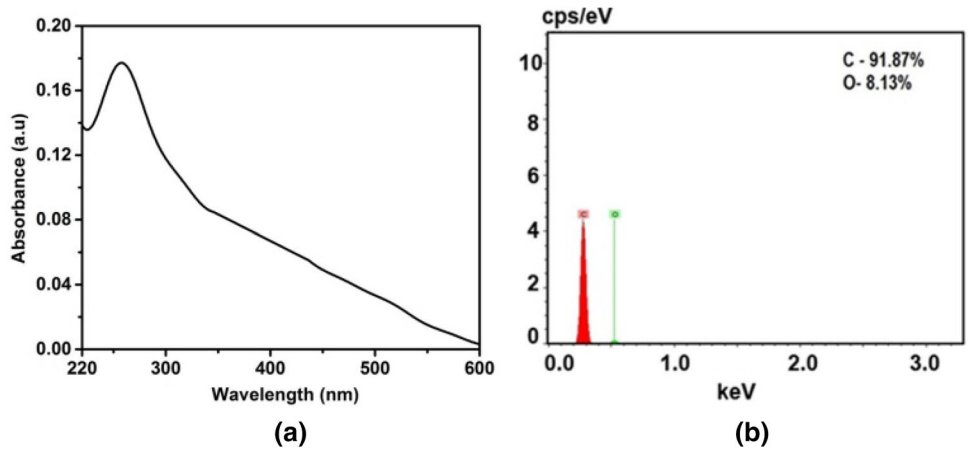

Fig. 7 **a** UV–visible and (**b**) EDS spectrum of sample T1

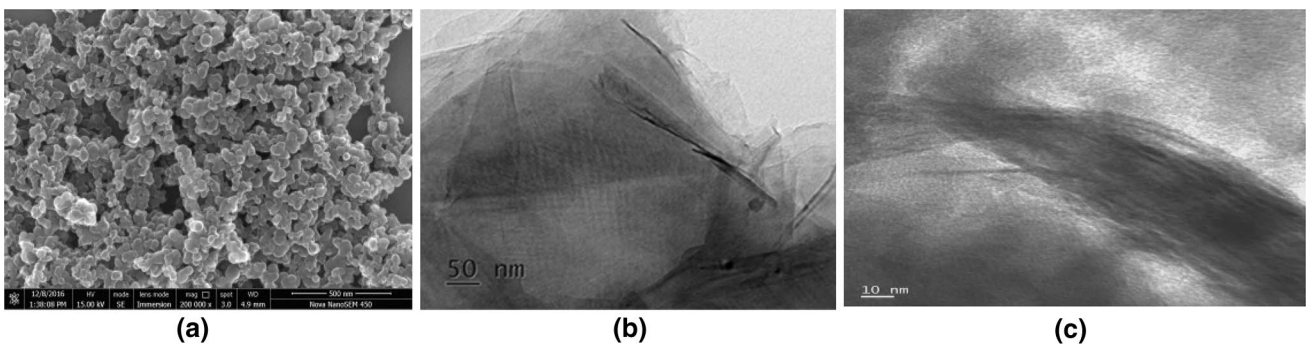

Fig. 8 **a** FESEM and (**b**, **c**) HR-TEM image of sample T5

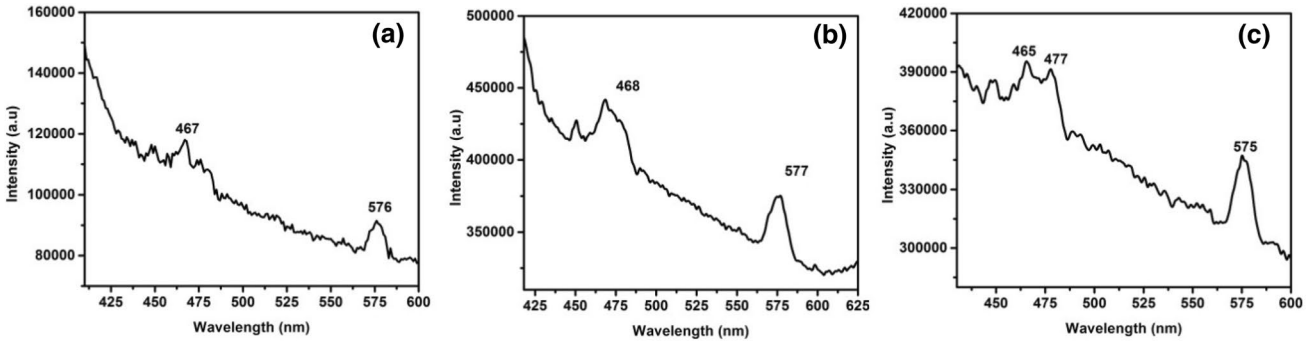

Fig. 9 PL spectrum of sample at (**a**) 30 °C (**b**) 200 °C(**c**) 400 °C for $\lambda_{exc} = 350$ nm

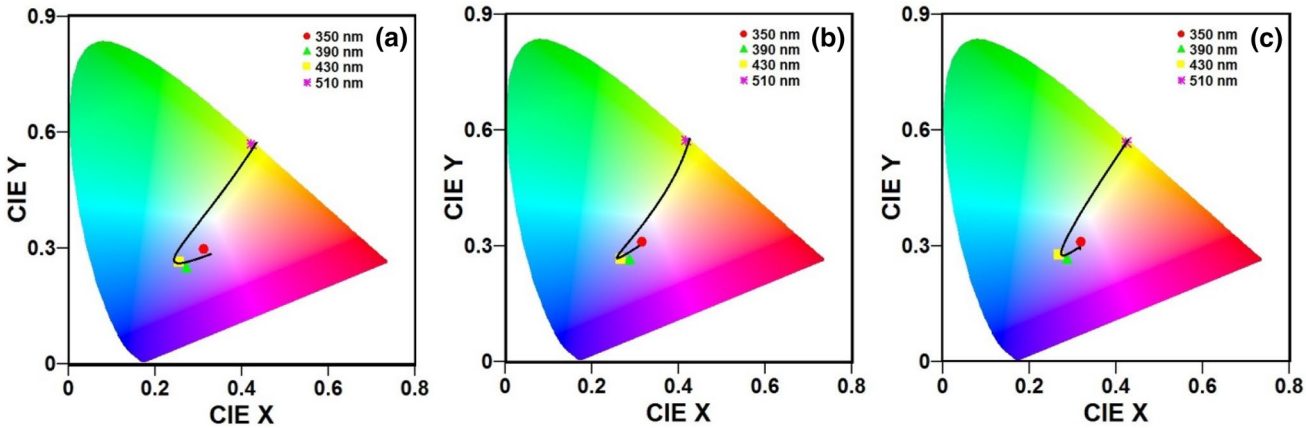

Fig. 10 CIE plot for the sample under different excitations and annealed at (**a**) 30 °C (**b**) 200 °C (**c**) 400 °C

data induces a tunable photoluminescent emission from the carbon nanosystem formed by the controlled combustion of gingelly oil. The non-uniform-sized particles and structural variations in the allotropic forms of carbon present in the soot sample as a result of annealing leads to the order–disorder–reorder transition which is responsible for the variations in the luminescence emission from the sample. For a material to be used as light emitters, its fluorescence quantum yield value should be high. It gives the ratio of photons emitted to the photons absorbed which is measured using integrating sphere method. In the present study, a good quantum yield value of 46.15% at an emission wavelength of 575 nm is obtained showing the possibility of the sample to be explored as energy-efficient light-emitting materials.

Conclusion

In the present study CNPs are synthesized by the controlled combustion of gingelly oil and the soot is analysed by XRD, EDS, FTIR, FESEM, HR-TEM, Raman, UV–visible and photoluminescent spectroscopic methods. The Raman spectra exhibit oscillatory order behaviour on annealing which is confirmed by the XRD analysis. The order fluctuation in the carbon nanosystem could be attributed to the thinning/shortening of MWCNTs, desorption of hydrogen and removal of amorphous carbon. The formation of CNTs is evident from the HR-TEM analysis. This oscillatory order pattern may be useful in designing materials with tunable luminescent behaviour and electrical conductivity. The PL spectrum, CIE plots, and colour purity help in understanding the annealing temperature-induced order fluctuation which in turn leads to the tunable light emission on photo excitation. Thus, the varying amount of CNTs in the soot, by annealing temperature, varies the luminescence property and makes it a low-cost tunable material for optoelectronic applications.

Acknowledgements The authors have no relevant financial interests in the paper and no other potential conflicts of interest to disclose.

Compliance with ethical standards

Conflicts of interest The authors declare that they have no conflict of interest.

References

1. Swapna, M.S., Saritha Devi, H.V., Sankararaman, S.: Camphor soot: a tunable light emitter. Appl. Phys. A. **124**, 50 (2018). https://doi.org/10.1007/s00339-017-1445-9
2. Murphy, H., Papakonstantinou, P., Okpalugo, T.I.T.: Raman study of multiwalled carbon nanotubes functionalized with oxygen groups. J. Vac. Sci. Technol. B Microelectron. Nanom. Struct. Process. Meas. Phenom. 24, 715–720 (2006)
3. Moon, J.S., Park, J.H., Lee, T.Y., Kim, Y.W., Yoo, J.B., Park, C.Y., Kim, J.M., Jin, K.W.: Transparent conductive film based on carbon nanotubes and PEDOT composites. Diam. Relat. Mater. **14**, 1882–1887 (2005)
4. Manoj, B., Kunjomana, A.G.: Chemical leaching of an Indian bituminous coal and characterization of the products by vibrational spectroscopic techniques. Int. J. Miner. Metall. Mater. **19**, 279–283 (2012)
5. Mohan, A.N., Manoj, B.: Synthesis and characterization of carbon nanospheres from hydrocarbon soot. Int. J. Electrochem. Sci. **7**, 9537–9549 (2012)
6. Krato, H.W., Heath, J.R.: O'Brien, SC, Curl, RF & Smalley. RE. Nature. **318**, 162–163 (1985)
7. Iijima, S.: Helical microtubules of graphitic carbon. Nature. **354**, 56 (1991)
8. Flahaut, E., Peigney, A., Laurent, C., Rousset, A.: Synthesis of single-walled carbon nanotube–Co–MgO composite powders and extraction of the nanotubes. J. Mater. Chem. **10**, 249–252 (2000)
9. Flahaut, E., Bacsa, R., Peigney, A., Laurent, C.: Gram-scale CCVD synthesis of double-walled carbon nanotubes. Chem. Commun. (2003). https://doi.org/10.1039/B301514A
10. Kumar, D., Verma, V., Dharamvir, K.: Elastic moduli of carbon nanotubes using second generation improved brenner potential. J. Nano Res. **15**, 1–10 (2011). https://doi.org/10.4028/www.scientific.net/JNanoR.15.1
11. Gupta, S., Dharamvir, K., Jindal, V.K.: Elastic moduli of single-walled carbon nanotubes and their ropes. Phys. Rev. B. **72**, 165428 (2005)
12. Swapna, M.S., Sankararaman, S.: Carbon nanonecklaces with carbon nanotubes and carbon dots. Int J Mater Sci. **12**, 541–548 (2017)
13. Chen, T., Dai, L.: Carbon nanomaterials for high-performance supercapacitors. Mater. Today. **16**, 272–280 (2013)
14. Ferrari, A.C., Robertson, J.: Interpretation of Raman spectra of disordered and amorphous carbon. Phys. Rev. B. **61**, 14095 (2000)
15. Matthews, M.J., Pimenta, M.A., Dresselhaus, G., Dresselhaus, M.S., Endo, M.: Origin of dispersive effects of the Raman D band in carbon materials. Phys. Rev. B. **59**, R6585 (1999)
16. Cançado, L.G., Takai, K., Enoki, T., Endo, M., Kim, Y.A., Mizusaki, H., Jorio, A., Coelho, L.N., Magalhaes-Paniago, R., Pimenta, M.A.: General equation for the determination of the crystallite size L a of nanographite by Raman spectroscopy. Appl. Phys. Lett. **88**, 163106 (2006)
17. Lehman, J.H., Terrones, M., Mansfield, E., Hurst, K.E., Meunier, V.: Evaluating the characteristics of multiwall carbon nanotubes. Carbon N. Y. **49**, 2581–2602 (2011)
18. Singh, D.K., Iyer, P.K., Giri, P.K.: Optical signature of structural defects in single walled and multiwalled carbon nanotubes. J. Nanosci. Nanotechnol. **9**, 5396–5401 (2009)
19. Fantini, C., Jorio, A., Souza, M., Saito, R., Samsonidze, G.G., Dresselhaus, M.S., Pimenta, M.A.: Steplike dispersion of the intermediate-frequency Raman modes in semiconducting and metallic carbon nanotubes. Phys. Rev. B. **72**, 85446 (2005)
20. Islam, S.S., Shah, K.A., Mavi, H.S., Shaukla, A.K., Rath, S.: Raman study on single-walled carbon nanotubes with different laser excitation energies. Bull. Mater. Sci. **30**, 295–299 (2007)
21. Swapna, M.S., Sankararaman, S.: Investigation of graphene oxide in diesel soot. J. Mater. Sci. Nanotechnol. **5**, 104 (2017)
22. Dresselhaus, M.S., Dresselhaus, G., Saito, R., Jorio, A.: Raman spectroscopy of carbon nanotubes. Phys. Rep. **409**, 47–99 (2005)
23. Swapna, M.S., Sankararaman, S.: Blue light emitting diesel soot for photonic applications. Mater. Res. Express. 5, 016203 (2018). doi:10.1088/2053-1591/aaa656
24. Swapna, M.S., Sankararaman, S.: From futile to fruitful: diesel soot as white light emitter. J. Fluoresc. **28**, 543–549 (2018). https://doi.org/10.1007/s10895-018-2215-6
25. Prasad, K.S., Fan, N., Wu, L., Chang, H., Wang, L., Hwang, K., Hwu, R.J., Horng, J., Lin, C., Ho, J.A.: A Tunable multicolor photoluminescent nanocarbon prepared from castor oil soot. J. Chinese Chem. Soc. **59**, 802–808 (2012)
26. Sun, Y., Li, S., Shang, Y., Hou, S., Chang, S., Shi, E., Cao, A.: Highly stretchable carbon nanotube fibers with tunable and stable light emission. Adv. Eng. Mater. **21**, 1801126 (2019). https://doi.org/10.1002/adem.201801126
27. Wei, J., Zhu, H., Wu, D., Wei, B.: Carbon nanotube filaments in household light bulbs. Appl. Phys. Lett. **84**, 4869–4871 (2004)
28. Zhang, Q., Chen, S., Zhang, S., Shang, W., Liu, L., Wang, M., Yu, H., Deng, L., Qi, G., Wang, L.: Negative differential resistance and hysteresis in graphene-based organic light-emitting devices. J. Mater. Chem. C. **6**, 1926–1932 (2018)
29. Xu, Q., Li, W., Ding, L., Yang, W., Xiao, H., Ong, W.-J.: Function-driven engineering of 1D carbon nanotubes and 0D carbon dots: mechanism, properties and applications. Nanoscale. **11**, 1475–1504 (2019)
30. Yao, Y., Jiang, F., Yang, C., Fu, K.K., Hayden, J., Lin, C.-F., Xie, H., Jiao, M., Yang, C., Wang, Y.: Epitaxial welding of carbon nanotube networks for aqueous battery current collectors. ACS Nano. **12**, 5266–5273 (2018)
31. Devi, H.V.S., Swapna, M.S., Raj, V., Ambadas, G., Sankararaman, S.: Optical emission diagnosis of boron carbide synthesized using natural carbon precursors. Opt. Spectrosc. **125**, 928–932 (2018). https://doi.org/10.1134/S0030400X18120251
32. Swapna, M.S., Devi, H.V.S., Ambadas, G., Sankararaman, S.: Fluorescent emission from a natural carbon matrix incorporating sodium. J. Mater. Sci. Mater. Electron. 1–10 (2018)
33. Swapna, M.S., Devi, H.V.S., Raj, V., Sankararaman, S.: Fractal and spectroscopic analysis of soot from internal combustion engines. Eur. Phys. J. Plus. **133**, 106 (2018)
34. Pang, L.S.K., Saxby, J.D., Chatfield, S.P.: Thermogravimetric analysis of carbon nanotubes and nanoparticles. J. Phys. Chem. **97**, 6941–6942 (1993)
35. Dunens, O.M., MacKenzie, K.J., Harris, A.T.: Synthesis of multiwalled carbon nanotubes on fly ash derived catalysts. Environ. Sci. Technol. **43**, 7889–7894 (2009)
36. Ajayan, P.M., Ebbesen, T.W., Ichihashi, T., Iijima, S., Tanigaki, K., Hiura, H.: Opening carbon nanotubes with oxygen and implications for filling. Nature. **362**, 522 (1993)

37. Yao, N., Lordi, V., Ma, S.X.C., Dujardin, E., Krishnan, A., Treacy, M.M.J., Ebbesen, T.W.: Structure and oxidation patterns of carbon nanotubes. J. Mater. Res. **13**, 2432–2437 (1998)
38. McKee, G.S.B., Flowers, J.S., Vecchio, K.S.: Length and the oxidation kinetics of chemical-vapor-deposition-generated multiwalled carbon nanotubes. J. Phys. Chem. C. **112**, 10108–10113 (2008)
39. Kim, D.-Y., Yun, Y.S., Kwon, S.-M., Jin, H.-J.: Preparation of aspect ratio-controlled carbon nanotubes. Mol. Cryst. Liq. Cryst. **510**, 79/[1213]–86/[1220] (2009). https://doi.org/10.1080/15421400903058338
40. Kim, D.Y., Yang, C.-M., Park, Y.S., Kim, K.K., Jeong, S.Y., Han, J.H., Lee, Y.H.: Characterization of thin multi-walled carbon nanotubes synthesized by catalytic chemical vapor deposition. Chem. Phys. Lett. **413**, 135–141 (2005). https://doi.org/10.1016/j.cplett.2005.07.064
41. Tuinstra, F., Koenig, J.: Lo: Raman spectrum of graphite. J. Chem. Phys. **53**, 1126–1130 (1970)
42. Nativ-Roth, E., Nap, R.J., Szleifer, I., Yerushalmi-Rozen, R.: Order–disorder transition induced by surfactant micelles in single-walled carbon nanotubes dispersions. Soft Matter. **6**, 5289–5292 (2010)
43. Singh, D.K., Iyer, P.K., Giri, P.K.: Distinguishing defect induced intermediate frequency modes from combination modes in the Raman spectrum of single walled carbon nanotubes. J. Appl. Phys. **111**, 64304 (2012)
44. He, X.Q., Kitipornchai, S., Wang, C.M., Liew, K.M.: Modeling of van der Waals force for infinitesimal deformation of multi-walled carbon nanotubes treated as cylindrical shells. Int. J. Solids Struct. **42**, 6032–6047 (2005)
45. Manoj, B.: Characterization of nano-crystalline carbon from camphor and diesel by x-ray diffraction technique. Asian J. Chem. **26**, 4553 (2014)
46. Shooto, N.D., Dikio, E.D.: Synthesis and characterization of diesel. Kerosene Candle Wax Soot's. **7**, 4335–4344 (2012)
47. Manoj, B., Kunjomana, A.G.: Structural characterization of selected Indian coals by X-ray diffraction and spectroscopic techniques. Trends Appl. Sci. Res. **7**, 434–444 (2012)
48. Ţucureanu, V., Matei, A., Avram, A.M.: FTIR spectroscopy for carbon family study. Crit. Rev. Anal. Chem. **46**, 502–520 (2016). https://doi.org/10.1080/10408347.2016.1157013
49. Dubey, P., Muthukumaran, D., Dash, S., Mukhopadhyay, R., Sarkar, S.: Synthesis and characterization of water-soluble carbon nanotubes from mustard soot. Pramana. **65**, 681–697 (2005). https://doi.org/10.1007/BF03010456
50. Yudianti, R.: Analysis of functional group sited on multi-wall carbon nanotube surface. Open Mater. Sci. J. **5**, 242–247 (2011). https://doi.org/10.2174/1874088X01105010242
51. Kouklin, N., Tzolov, M., Straus, D., Yin, A., Xu, J.M.: Infrared absorption properties of carbon nanotubes synthesized by chemical vapor deposition. Appl. Phys. Lett. **85**, 4463 (2004). https://doi.org/10.1063/1.1812837
52. Rance, G.A., Marsh, D.H., Nicholas, R.J., Khlobystov, A.N.: UV–vis absorption spectroscopy of carbon nanotubes: relationship between the π-electron plasmon and nanotube diameter. Chem. Phys. Lett. **493**, 19–23 (2010)